

MammoDL: Mammographic Breast Density Estimation using Federated Learning

Ramya Muthukrishnan¹, Angelina Heyler², Keshava Katti², Sarthak Pati^{3,4,5}, Walter Mankowski^{3,5}, Aprupa Alahari¹, Michael Sanborn², Emily F. Conant⁵, Christopher Scott⁶, Stacey Winham⁶, Celine Vachon⁶, Pratik Chaudhari¹, Despina Kontos^{3,5*}, Spyridon Bakas^{3,4,5*}.

Affiliations:

¹Department of Computer and Information Science, University of Pennsylvania, Philadelphia, PA, USA.

²Department of Electrical and Systems Engineering, University of Pennsylvania, Philadelphia, PA, USA.

³Center for Biomedical Image Computing and Analytics (CBICA), University of Pennsylvania, Philadelphia, PA, USA.

⁴Department of Pathology & Laboratory Medicine, Perelman School of Medicine, University of Pennsylvania, Philadelphia, PA, USA.

⁵Department of Radiology, Perelman School of Medicine, University of Pennsylvania, Philadelphia, PA, USA.

⁵Department of Health Sciences Research, Mayo Clinic, Rochester, MN, USA.

*Corresponding authors. Email: despina.kontos@pennmedicine.upenn.edu, sbakas@upenn.edu.

Abstract: Assessing breast cancer risk from imaging remains a subjective process, in which radiologists employ simple computer aided detection (CAD) systems or qualitative visual assessment to estimate breast percent density (PD). Machine learning (ML) models have become the most promising way to quantify breast cancer risk for early, accurate, and equitable diagnoses, but training such models in medical research is often restricted to small, single-institution data. Since patient demographics and imaging characteristics may vary considerably across imaging sites, models trained on single-institution data tend not to generalize well. In response to this problem, MammoDL is proposed, an open-source software tool that leverages a U-Net architecture to accurately estimate breast PD and complexity from mammography. With the Open Federated Learning (OpenFL) library, this solution enables secure training on datasets across multiple institutions. MammoDL is a leaner, more flexible model than its predecessors, boasting improved generalization due to federation-enabled training on larger, more representative datasets.

One-Sentence Summary: MammoDL uses the U-Net deep learning architecture to quantitatively assess breast tissue density and complexity from mammograms and enables a data privacy approach by using federated learning.

Keywords: Breast Cancer Risk, Mammography, Breast Density, Deep Learning, Machine Learning, Federated Learning, OpenFL.

1. Introduction

Breast cancer remains the most frequent cancer among women, with about 1 in 8 women in the United States developing breast cancer over the course of her lifetime [1]. Furthermore, breast cancer is the most common cause of cancer-related death for women worldwide [2]. The goal of mammographic screening is to reduce the mortality rate of breast cancer. As such, mammography has become the most standard and reliable method for breast screening today. Randomized trials and incidence-based mortality studies show a notable decrease in breast cancer mortality due to participation in mammography screenings [3-5]. In particular, mammography is highly effective in identifying breast cancers before they become fatal [6]. While mammography may be widely considered as the gold standard of breast screening, it suffers from relatively poor sensitivities ranging from 75% to 85%, with the lowest sensitivity in detecting cancers in women with the densest breast tissue [7]. Mammography screenings consist of two-view (mediolateral oblique (MLO) and craniocaudal (CC)) bilateral examinations captured as full-field digital mammography (FFDM) images. In the United States, a large portion of screenings are also with digital breast tomosynthesis (DBT), which capture a 3-dimensional image of the breast, but this technique still suffers from diminished sensitivity as breast density increases. Radiologists then perform a visual grading of breast density based on the American College of Radiology's Breast Imaging Reporting and Data Systems (BI-RADS). Some radiologists employ simple computer-aided detection (CAD) systems, which generally present limited improvements [8], especially in comparison to their machine learning (ML) counterparts.

Breast density not only limits the sensitivity of mammographic screenings but is also a major risk factor for breast cancer [9]. Over 43% of women in the United States between the age of 40 to 74 have heterogeneously or extremely dense breasts [10]. The most frequent method to grade breast density is subjective, using the BI-RADS classification of breast density based on mammographic images [10-12]. This method does not provide a continuous, real-valued percent density (PD), which would help a radiologist better monitor changes in a patient's breast density that point to heightened breast cancer risk, but rather classifies the breast into one of four density categories.

Current efforts to automate quantitative breast density estimates from mammographic images come in the form of commercially available software and research tools. The semi-automated thresholding tool Cumulus remains the current gold-standard area-based breast density estimation method for breast cancer screenings. Commercial software for volumetric breast composition measurement, like Quantra [13] and Volpara [14], show strong association with Cumulus [15] but with several key limitations. These tools determine breast density from x-ray beam interaction models, which make underlying assumptions on metadata to simplify estimates that can lead to inaccurate results [9], especially if some of the prerequisite metadata is not available. Such commercial software may be expensive and may suffer from limited interpretability, as the tools do not output a spatial map delineating the dense tissue from the non-dense tissue in the mammogram. Research tools [16-28] come with their own set of limitations. First, with the exception of LIBRA, such tools are not freely available, which not only decreases their likelihood of adoption but also the ability to benchmark their performance with other available PD estimation methods. Second, these research tools have been trained on small, single-institution datasets [9], a consequence of the data silo problem that plagues the medical imaging field.

Upon the advent of deep learning (DL), convolutional neural networks (CNN) have become the workhorse for fully automated mammographic density estimation tools [8]. Such algorithms rely on sufficiently large and diverse datasets for training, but these datasets can be tremendously difficult to obtain in the medical field. Furthermore, single-institution datasets are

not sufficient to provide a representative sample for model training and can lead to low-accuracy generalization [29]. In addition, multi-institutional collaborations that employ centrally shared patient data present numerous privacy and ownership concerns. The solution to these concerns is a novel paradigm for multi-site collaboration called federated learning [29], which allows model training to leverage data across multiple decentralized institutions without sharing data between institutions. Instead, the training process is distributed to each of the data owners and then aggregated into a single model, which not only addresses access rights and privacy concerns from multi-institutional collaborations but vastly increases the generalizability of DL-based medical imaging models as compared to collaborative data sharing (CDS) [29].

This work presents MammoDL, a breast PD estimation tool that builds upon Deep-LIBRA [9], a DL-based improvement to the Laboratory for Individualized Breast Radiodensity Assessment (LIBRA) tool [16]. MammoDL utilizes 2 deep learning models (U-Nets) to separately segment the breast and dense tissue regions from the mammogram in order to accurately estimate PD. In contrast to Deep-LIBRA, which uses separate U-Nets to remove the background and to remove the pectoralis muscle, MammoDL uses one U-Net to do both by directly segmenting the breast in the mammogram. Furthermore, while Deep-LIBRA segments the dense tissue using traditional ML modeling, particularly a support vector machine (SVM), MammoDL replaces this step with deep learning by employing a U-Net to perform this segmentation. Thus, MammoDL is a fully DL-based pipeline for PD estimation that is more lightweight and flexible than Deep-LIBRA. Lastly, MammoDL leverages federated learning capabilities offered by the Open Federated Learning (OpenFL) library [30] to increase the accuracy and generalizability of breast PD estimation with respect to the ground-truth labels produced by a “gold-standard” Cumulus reader. It should be noted that MammoDL is designed to be a hybrid model that combines an ML algorithm with a radiologist assessment, which is shown to be more effective than either of the two operating independently [31].

2. Materials and Methods

MammoDL was conceived as the solution to three different problems facing the broader breast cancer risk assessment community. First, ML-based breast PD estimation tools tended to include numerous segmentation steps or classification/regression tasks, leading to overly complex models that would either generalize poorly or present significant computational costs that limited their usefulness. As a result, the goal was for MammoDL to be a lean ML model with comparable accuracy to its predecessor, Deep-LIBRA. Feature pyramids to detect objects at different scales [32] have already penetrated the medical imaging space, with examples like multi-class segmentation in chest radiographs [33], which motivated MammoDL to execute a multi-segmentation task that offered better generalization to new mammogram images (Fig. 1b). Second, the problem of small, single-institution training datasets was addressed by incorporating a federated learning pipeline into MammoDL, a measure taken to further enhance model generalization (Fig. 1a). Finally, we have made MammoDL freely available on GitHub for all those interested in the code and models related to this work.

2.1. Study Datasets

The dataset used for model training and validation (Table 1) consisted of negative FFDM screening exams obtained from the Hospital of the University of Pennsylvania (HUP), Philadelphia, PA, and the Mayo Clinic (MC), Rochester, MN [9]. It included 6,713 bilateral CC-view images from 1,679 women from the MC and 1,147 bilateral MLO-view images from 575 women from HUP. The ground-truth PD labels were curated on Cumulus by a “gold-standard” (> 20 years of experience estimating PD with Cumulus) human reader. The holdout test dataset

consisted of similar data from HUP and the MC; it consisted of 278 MLO-view images from 110 women at HUP and 6463 bi-lateral CC and MLO images from 1628 women at the MC. The HUP data is racially diverse, which is an important dataset characteristic to accurately assess breast PD [34].

In preparation for the multi-segmentation task, all images were labeled with breast masks such that Class 0 corresponded to the background and pectoralis muscle, while Class 1 corresponded to the breast. What remained was the portion of the mammogram containing only the breast, which acted as the input for the second segmentation model, in which Class 0 corresponded to the non-dense tissue, while Class 1 corresponded to the dense tissue.

2.2. Data Pre-Processing

Each original mammogram, stored as DICOM images, was pre-processed by removing the metal tag in the image, down-sampling the images to ensure a standardized shape across the cohort (i.e., 512x512), rescaling pixel intensities to [0,1] using min-max scaling, and removing the metal tag in the mammogram. These images are the inputs to the breast segmentation model during both training and inference (Fig. 3a). The inputs to the dense tissue segmentation model are further pre-processed by removing non-breast pixels (determined by the manual breast mask during training and the predicted breast mask during inference) and re-normalizing pixel values with min-max scaling (Fig. 3c).

2.3. Model Architecture

Due to the wide use of residual connections in many state-of-the-art neural network architectures and their contributions to breakthroughs in computer vision, the ResNet [35] was selected for this medical imaging task. ResNet architecture not only eases the challenges of training deep neural networks (e.g., by avoiding the vanishing gradient and degradation problems) but boasts outstanding generalization to new data points [36]. The ResNet is employed as the encoder for a U-Net, [37] a widely used segmentation module that operates by first down-sampling and then up-sampling an image, creating the “U”-like shape for which it is named. The specific ResNet architecture selected was the ResNet34, and the weights were obtained from pre-training on ImageNet data [38]. Modifying the U-Net with a pre-trained ResNet34 encoder (Fig. 2) brings the aforementioned ResNet architecture advantages to the segmentation task plus an increase in the speed of training due to the ability to obtain pre-trained ResNet encoders [39]. MammoDL consists of two such modified U-Nets, the first for identifying the breast from the entire mammogram and the second for delineating the dense tissue region from the breast.

During evaluation and inference, predicted segmentations from each U-Net are resampled to the original image size. The number of pixels in each predicted segmentation are calculated as a measure of area, with the area of the dense tissue region divided by the area of the breast region to return the breast PD (Fig. 3d).

2.4. Federated Learning

The primary motivation for training the MammoDL model in a federated manner was to expand the size and diversity of the medical training data and facilitate multi-institutional collaborations without having to share the data among institutions [29, 38, 40-42]. In the field of medical imaging, the impact of federated learning to a ML-based model cannot be understated, with its addition increasing generalization accuracy by up to 35% [42]. In the aggregator-server federated learning framework [38], each participant contributing model updates using their own data is known as a collaborator, with a single aggregator node combining these model updates into a single consensus model. For the purpose of this work, collaborator nodes are hospitals that own

a dataset of FFDM images in which the dense breast tissue is labeled. The DL model is trained locally at each collaborator node for a specified number of epochs. The aggregator node is connected to the collaborator nodes by remote procedure calls (gRPC). OpenFL enables these calls to occur via a mutually authenticated transport layer security (TLS) network connection. Through this secure channel, the collaborator nodes pass tasks, model and optimizer weights, and other metrics in order for the aggregator node to combine the model weights to construct a global consensus model, which is then passed back to the collaborator nodes. Each such process is a “federated training round”, and continues for preset number of rounds.

OpenFL was used to simulate a federated learning scenario, where the MC and HUP were collaborator nodes in independent compute processes. To avoid cross-institutional data sharing, the model weights were aggregated across all datasets by taking a weighted average of updates after each epoch, where the weights were proportional to the dataset size. OpenFL ensured that the multi-institutional collaborations were secure, especially for those ML model builders who seek to protect their model intellectual property or those data holders who wish to uphold the privacy of their information [30].

2.5. Model Training and Development

Both U-Nets were trained with the same hyperparameters. They were trained with a batch size of 16, a learning rate of $1e-4$, and weight decay of $1e-4$. The models trained for 30 epochs with the Adam optimizer. Data augmentation (random horizontal and vertical flipping of images) was used to improve model generalization. The entire dataset was randomly split into training and validation datasets using a 4:1 ratio, respectively. Validation performance was used for hyperparameter optimization; thus, the model is evaluated on a holdout test dataset in addition to the validation dataset to provide a fair assessment of algorithm performance.

2.6. Model Evaluation

The MammoDL algorithm was evaluated by calculating the mean absolute error (MAE) between the true and predicted percent density values across the test data. MAE was chosen over mean squared error (MSE), or root mean squared error (RMSE) for its interpretability to clinicians, as MAE directly estimates the average error of the model in its percent density prediction. However, MAE does not provide a full picture of algorithm performance because it does not spatially capture segmentation accuracies. Thus, the Dice-Sorensen coefficient (DSC) [43], a widely used performance metric for segmentation tasks [44], was used to evaluate the performance of the individual segmentation models. DSC essentially measures the area of overlap between ground-truth segmentations X and algorithmic segmentations Y . It is computed by the equation $DSC = \frac{2|X \cap Y|}{|X| + |Y|}$. The DSC value ranges from 0 to 1, with 1 perfect overlap of the ground truth and predicted segmentations. Reported DSC values are averaged across images.

2.7. Code Availability

All of the work described here is freely available for those who would like to iterate and improve upon this algorithm via our GitHub page <https://github.com/ramyamut/MammoDL>.

3. Results

3.1. Evaluation on validation dataset

The model trained on both datasets using a standard centralized training scheme resulted in PD MAEs of 3.7918 and 3.9711, breast segmentation DSCs of 0.9896 and 0.9813, and dense

tissue segmentation DSCs of 0.7755 and 0.7078, on the MC and HUP validation datasets, respectively. The model trained on both datasets using our federated training scheme resulted in PD MAEs of 3.9740 and 4.2811, breast segmentation DSCs of 0.9880 and 0.9727, and dense tissue segmentation DSCs of 0.7634 and 0.6787, on the MC and HUP development datasets, respectively. The models trained on single-institution datasets had much worse performance metrics than the models trained on both datasets (Table 2).

3.2. Evaluation on independent test dataset

The model trained on both datasets using a standard centralized training scheme resulted in PD MAEs of 3.8616 and 3.9937, breast segmentation DSCs of 0.9893 and 0.9722, and dense tissue segmentation DSCs of 0.7745 and 0.6879, on the MC and HUP test datasets, respectively. The model trained on both datasets using our federated training scheme resulted in PD MAEs of 3.9586 and 4.2409, breast segmentation DSCs of 0.9881 and 0.9657, and dense tissue segmentation DSCs of 0.7637 and 0.6417, on the MC and HUP test datasets, respectively. The models trained on single-institution datasets expectedly performed much worse than the models that utilized both datasets for development (Table 3).

4. Discussion

The results suggest that there is a demonstrated need to train on multi-institutional datasets, as models trained on both HUP and MC data significantly outperform those trained on either HUP or MC data only. Additionally, we have shown that models trained on solely HUP or MC data tended not to generalize well to data from other sources. Furthermore, the model trained with federated learning achieved nearly the same performance as the model trained with a standard centralized training scheme, demonstrating that our federated model is robust, and that federated learning can be used to solve the problem of breast PD estimation.

The generalization performance of the MammoDL model is compared with that of some breast PD estimation tools mentioned in the introduction of this work. Even with an optimized cutoff value for risk stratification, Quantra suffers from a sensitivity of 65% and a specificity of 77% when performing BI-RADS classification, where scores of D3/D4 denote high-risk densities and D1/D2 denote low-risk densities [45]. As Volpara requires the same metadata as Quantra, these software tools tend to behave similarly [9], while the outputs of semi-automated thresholding tools, like Cumulus, are known to vary noticeably based on the expertise of the individual operating the tool [11]. As a result, MammoDL and Deep-LIBRA are the standout performers when it comes to generalization to unseen mammogram images, with both models boasting strong testing accuracy metrics. The MAE for the PD estimates of MammoDL are lower than those reported by Deep-LIBRA and LIBRA (Fig. 4). However, the crucial difference between MammoDL and Deep-LIBRA is that MammoDL offers a federated learning pipeline that, when trained on more than HUP and MC data, will exhibit even better performance due to learning from larger, more diverse training data. Furthermore, MammoDL is a leaner, more flexible model that requires fewer segmentation steps and no non-DL classifiers.

In the future, the goal is to incorporate datasets from more institutions to further validate the robustness of this model and its federated training algorithm across diverse populations, as well as to integrate the training pipeline into a larger framework, such as the Generally Nuanced Deep Learning Framework (GaNDLF) [46], which would allow for wider distribution, more robust training (by leveraging a standardized set of pre-processing, augmentation, anonymization, and DL architectures), and easier hardware-independent deployment. In addition, we hope to bridge this gap by creating a user interface for clinicians to easily use our tool for breast cancer risk

assessment. This user interface is still in development and hence is only discussed in the conclusion of this work.

5. Conclusion

A deep learning pipeline was implemented to calculate breast PD from input mammograms. The MammoDL model produces a validation MAE of less than 5% and an interpretable spatial map showing the segmented breast and dense tissue regions that clinicians value over black-box predictions. A robust federated training capability was presented that preserves privacy while maintaining the benefits of training on multi-institutional datasets, enabled by OpenFL. We have made our code publicly available on GitHub in hopes that our tool will accelerate breast cancer research and clinical care.

References and Notes

1. Howlader N., Noone A.M., Krapcho M., Miller D., Brest A., Yu M., Ruhl J., Tatalovich Z., Mariotto A., Lewis D.R., Chen H.S., Feuer E.J., Cronin K.A. SEER Cancer Statistics Review, 1975-2016, *National Cancer Institute* (2019).
2. Lauby-Secretan, B., Scoccianti, C., Loomis, D., Benbrahim-Tallaa, L., Bouvard, V., Bianchini, F., Straif, K. Breast-Cancer Screening — Viewpoint of the IARC Working Group. *New England Journal of Medicine* **372** (24) (2015).
3. Tabar, L., Vitak, B., Chen, T.H., Yen, A.M., Cohen, A., Tot, T., Chiu, S.Y., Chen, S.L., Fann, J.C., Rosell, J., Fohlin, H., Smith, R.A., Duffy, S.W. Swedish two-county trial: impact of mammographic screening on breast cancer mortality during 3 decades. *Radiology* **260**, 658-663 (2011).
4. IARC Working Group on the Evaluation of Cancer-Preventive Strategies. *Breast Cancer Screening* **15**, IARC Press (2016).
5. Njor, S., Nystrom, L., Moss, S., Paci, E., Broeders, M., Segnan, N., Lynge, E., Euroscreen Working Group. Breast cancer mortality in mammographic screening in Europe: a review of incidence-based mortality studies. *Journal of Medical Screening* **19**, 33-41 (2012).
6. Duffy, S.W., Tabár, L., Yen, A.M.-F., Dean, P.B., Smith, R.A., Jonsson, H., Törnberg, S., Chen, S.L.-S., Chiu, S.Y.-H., Fann, J.C.-Y., Ku, M.M.-S., Wu, W.Y.-Y., Hsu, C.-Y., Chen, Y.-C., Svane, G., Azavedo, E., Grundström, H., Sundén, P., Leifland, K., Frodis, E., Ramos, J., Epstein, B., Åkerlund, A., Sundbom, A., Bordás, P., Wallin, H., Starck, L., Björkgren, A., Carlson, S., Fredriksson, I., Ahlgren, J., Öhman, D., Holmberg, L., Chen, T.H.-H. Mammography screening reduces rates of advanced and fatal breast cancers: Results in 549,091 women. *Cancer* **126**, 2971-2979 (2020).
7. Domingo, L., Hofvind, S., Hubbard, R.A., Roman, M., Benkeser, D., Sala, M., Castells, X. Cross-national comparison of screening mammography accuracy measures in U.S., Norway, and Spain. *European Radiology* **26**, 2520-2528 (2016).
8. Maghsoudi, O.H., Gastounioti, A., Scott, C., Pantalone, L., Wu, F., Cohen, E.A., Winham, S., Conant, E.F., Vachon, C., Kontos, D. Deep-LIBRA: An artificial-intelligence method for robust quantification of breast density with independent validation in breast cancer risk assessment. *Medical Image Analysis* **73**, 102138 (2021).
9. Sprague, B.L., Gangnon, R.E., Burt, V., Trentham-Deitz, A., Hampton, J.M., Wellman, R.D., Kerlikowske, K., Miglioretti, D.L. Prevalence of mammographically dense breasts in the United States. *Journal of the National Cancer Institute* **106** (10) (2014).

10. Sprague, B.L., Conant, E.F., Onega, T., Garcia, M.P., Beaber, E.F., Herschorn, S.D., Lehman, C.D., Tosteson, A.N.A., Lacson, R., Schnall, M.D., Kontos, D., Haas, J.S., Weaver, D.L., Barlow, W.E., PROSPR Consortium. Variation in mammographic breast density assessments among radiologists in clinical practice: a multicenter observational study. *Annals of Internal Medicine* **165** (7), 457-464 (2016).
11. Irshad, A., Leddy, R., Ackerman, S., Cluver, A., Pavic, D., Abid, A., Lewis, M.C. Effects of changes in BI-RADS density assessment guidelines (fourth versus fifth edition) on breast density assessment: intra-and interreader agreements and density distribution. *American Journal of Roentgenology* **207** (6), 1366-1371 (2016).
12. Bitencourt, A., Naranjo, I.D., Lo Gullo, R., Saccarelli, C.R., Pinker, K. AI-enhanced breast imaging: Where are we and where are we heading? *European Journal of Radiology* **142**, 109882 (2021).
13. Hartman, K., Highnam, R., Warren, R., Jackson, V. Volumetric Assessment of Breast Tissue composition from FFDM Images. *International Workshop on Digital Mammography* **5116**, 33-39 (2008).
14. Highnam, R., Brady, S.M., Yaffe, M.J., Karssemijer, N., Harvey, J. Robust Breast Composition Measurement. *International Workshop on Digital Mammography* **6136**, 378-385 (2010).
15. Kontos, D. Bakic, P.R., Acciavatti, R.J., Conant, E.F., Maidment, A.D.A. A Comparative Study of Volumetric and Area-Based Breast Density Estimation in Digital Mammography: Results from a Screening Population. *International Workshop on Digital Mammography* **6136**, 378-385 (2010).
16. Keller, B.M., Nathan, D.L., Wang, Y., Zheng, Y., Gee, J.C., Conant, E.F., Kontos, D. Estimation of breast percent density in raw and processed full field digital mammography images via adaptive fuzzy c-means clustering and support vector machine segmentation. *Medical Physics* **38** (8), 4903-4917 (2012).
17. Mustra, M., Grgic, M., Rangayyan, R.M. Review of recent advances in segmentation of the breast boundary and the pectoral muscle in mammograms. *Medical & Biological Engineering & Computing* **54**, 1003-1024 (2016).
18. Li, Y., Chen, H., Yang, Y., Yang, N. Pectoral muscle segmentation in mammograms based on homogenous texture and intensity deviation. *Pattern Recognition* **46** (3), 681-691 (2013).
19. Shi, P., Zhong, J., Rampun, A., Wang, H. A hierarchical pipeline for breast boundary segmentation and calcification detection in mammograms. *Computers in Biology and Medicine* **96**, 178-188 (2018).
20. Anitha, J., Peter, J.D., Pandian, S.I.A. A dual stage adaptive thresholding (DuSAT) for automatic mass detection in mammograms. *Computer Methods and Programs in Biomedicine* **138**, 93-104 (2017).
21. Ferrari, R.J., Rangayyan, R.M., Desautels, J.E.L., Borges, R.A., Frere, A.F. Automatic identification of the pectoral muscle in mammograms. *IEEE Transactions on Medical Imaging* **23** (2), 232-245 (2004).
22. Kwok, S.M., Chandrasekhar, R., Attikiouzel, Y., Rickard, M.T. Automatic pectoral muscle segmentation on mediolateral oblique view mammograms. *IEEE Transactions on Medical Imaging* **23** (9), 1129-1140 (2004).
23. Mustra, M., Grgic, M. Robust automatic breast and pectoral muscle segmentation from scanned mammograms. *Signal Processing* **93** (10), 2817-2827 (2013).
24. Nagi, J., Kareem, S.A., Nagi, F., Ahmed, S.K. Automated breast profile segmentation for ROI detection using digital mammograms. *2010 IEEE EMBS Conference on Biomedical Engineering and Sciences (IECBES)*. IEEE, 87-92 (2010).

25. Taghanaki, S.A., Liu, Y., Miles, B., Hamarneh, G. Geometry-based pectoral muscle segmentation from MLO mammogram views. *IEEE Transactions on Biomedical Engineering* **64** (11), 2662-2671 (2017).
26. Rampun, A., Morrow, P.J., Scotney, B.W., Winder, J. Fully automated breast boundary and pectoral muscle segmentation in mammograms. *Artificial Intelligence in Medicine* **79**, 28-41 (2017).
27. Czaplicka, K., Włodarczyk, J. Automatic breast-line and pectoral muscle segmentation. *Schedae Informaticae* **20** (2011).
28. Dembrower, K., Liu, Y., Azizpour, H., Eklund, M., Smith, K., Lindholm, P., Strand, F. Comparison of a deep learning risk score and standard mammographic density score for breast cancer risk prediction. *Radiology* **294** (2), 265-272 (2020).
29. Sheller, M.J., Edwards, B., Reina, G.A., Martin, J., Pati, S., Kotrotsou, A., Milchenko, M., Xu, W., Marcus, D. Colen, R.R., Bakas, S. Federated learning in medicine: facilitating multi-institutional collaborations without sharing patient data. *Scientific Reports* **10**, 12598 (2020).
30. Reina, G.A., Gruzdev, A., Foley, P., Perepelkina, O., Sharma, M., Davidyuk, I., Trushkin, I., Radionov, M., Mokrov, A., Agapov, D., Martin, J., Edwards, B., Sheller, M.J., Pati, S., Moorthy, P.N., Wang, S., Shah, P., Bakas, S. OpenFL: An open-source framework for Federated Learning. *arXiv* (2021).
31. Rodríguez-Ruiz, A., Krupinski, E., Mordang, J., Schilling, K., Heywang-Kobrunner, S.H., Sechopoulos, I., Mann, R.M. Detection of breast cancer with mammography: effect of an artificial intelligence support system. *Radiology* **290**, 305–314 (2019).
32. Lin, T., Dollar, P., Girshick, R., He, K., Hariharan, B., Belongie, S. Feature Pyramid Networks for Object Detection. *arXiv* (2017).
33. Novikov, A.A., Lenis, D., Major, D., Hladuvka, J., Wimmer, M., Buhler, K. Fully Convolutional Architectures for Multiclass Segmentation in Chest Radiographs. *IEEE Transactions on Medical Imaging* **37** (8), 1865-1876 (2018).
34. McCarthy, A.M., Keller, B.M., Pantalone, L.M., Hsieh, M.-K., Synnestvedt, M., Conant, E.F., Armstrong, K., Kontos, D. Racial differences in quantitative measures of area and volumetric breast density. *Journal of the National Cancer Institute* **108** (10), djw104 (2016).
35. He, K., Zhang, X., Ren, S., Sun, J. Deep residual learning for image recognition. *Proceedings of the IEEE Conference on Computer Vision and Pattern Recognition (CVPR)*, 770-778 (2016).
36. He, F., Liu, T., Tao, D. Why ResNet Works? Residuals Generalize. *IEEE Transactions on Neural Networks and Learning Systems* **31** (12), 5349-5362 (2020).
37. Ronneberger, O., Fischer, P., Brox, T. U-Net: convolutional networks for biomedical image segmentation. *International Conference on Medical Image Computing and Computer-Assisted Intervention*, 234-241 (2015).
38. Reike, N., Hancox, J., Li W., Milletari, F., Roth, H.R., Albarqouni, S., Bakas, S., Galtier, M.N., Landman, B.A., Maier-Hein, K., Ourselin, S., Sheller, M., Summers, R.M., Trask, A., Xu, D., Baust, M., Cardoso, M.J. The future of digital health with federated learning. *npj Digital Medicine* **3** (119), (2020).
39. Jalali, Y., Fateh, M., Rezvani, M., Abolghasemi, V., Anisi, M.H. ResBCDU-Net: A Deep Learning Framework for Lung CT Image Segmentation. *Sensors (Basel)* **21** (1), 268 (2021).
40. Pati, S., Baid, U., Edwards, B., Sheller, M., et al. Federated Learning Enables Big Data for Rare Cancer Boundary Detection. *arXiv* (2022).
41. Pati, S., Baid, U., Zenk, M., Edwards, B., Sheller, M., Reina, G.A., et al. The Federated Tumor Segmentation (FeTS) Challenge. *arXiv* (2021).

42. Baid, U., Pati, S., Thakur, S., Edwards, B., Sheller, M., Martin, J., Bakas, S. Federated Tumor Segmentation (FeTS) Initiative: The First Large-Scale Real-World Federation. *Neuro-Oncology* **23** (6), 135-136 (2021).
43. Zijdenbos, A.P., Dawant, B.M., Margolin, R.A., Palmer, A.C. Morphometric analysis of white matter lesions in MR images: method and validation. *IEEE Transactions on Medical Imaging* **13** (4), 716-725, (1994).
44. Maier-Hein, L., Reinke, A., Godau, P., Tizabi, M.D., et al. Metrics reloaded: Pitfalls and recommendations for image analysis validation. *arXiv* (2022).
45. Richard-Davis, G., Whittemore, B., Disher, A., Rice, V.M., Lenin, R.B., Dollins, C., Siegel, E.R., Eswaran, H. Evaluation of Qantra Hologic Volumetric Computerized Breast Density Software in Comparison With Manual Interpretation in a Diverse Population. *Breast Cancer: Basic and Clinical Research* **12** (2018).
46. Pati, S., Thakur, S.P., Bhalerao, M., Thermos, S., Baid, U., Gotkowsi, K., Gonzalez, C., Guley, O., Hamamci, I.E., Er, S., Grenko, C., Edwards, B., Sheller, M., Agraz, J., Baheti, B., Bashyam, V., Sharma, P., Haghighi, B., Gastounioti, A., Bergman, m. Mukhopadhyay, A., Tsaftaris, S.A., Menze, B., Kontos, D., Davatzikos, C., Bakas, S. GaNDLF: A Generally Nuanced Deep Learning Framework for Scalable End-to-End Clinical Workflows in Medical Imaging. *arXiv* (2021).

Acknowledgments: This work was supported in part by the University of Pennsylvania Department of Electrical and Systems Engineering Senior Design Fund.

Author Contributions: *Ramya Muthukrishnan:* Primary code development, data preprocessing, performance metric calculations, writing (final draft). *Angelina Heyler:* Federated learning pipeline development, performance metric calculations. *Keshava Katti:* Writing (original draft), initial code development. *Sarthak Pati:* Support with OpenFL, writing (review/editing). *Walter Mankowski:* data procurement. *Aprupa Alahari:* Development of user interface for clinical use. *Michael Sanborn:* Development of user interface for clinical use. *Emily F. Conant:* Radiologist insight, user testing. *Pratik Chaudhari:* Advisor for DL model selection. *Spyridon Bakas:* Conceptualization of federated learning components, computation resources, writing (review/editing), supervision, project administration. *Despina Kontos:* Conceptualization of breast PD estimation model, computation resources, writing (review/editing), supervision, project administration.

Competing interests: The authors declare no competing interests.

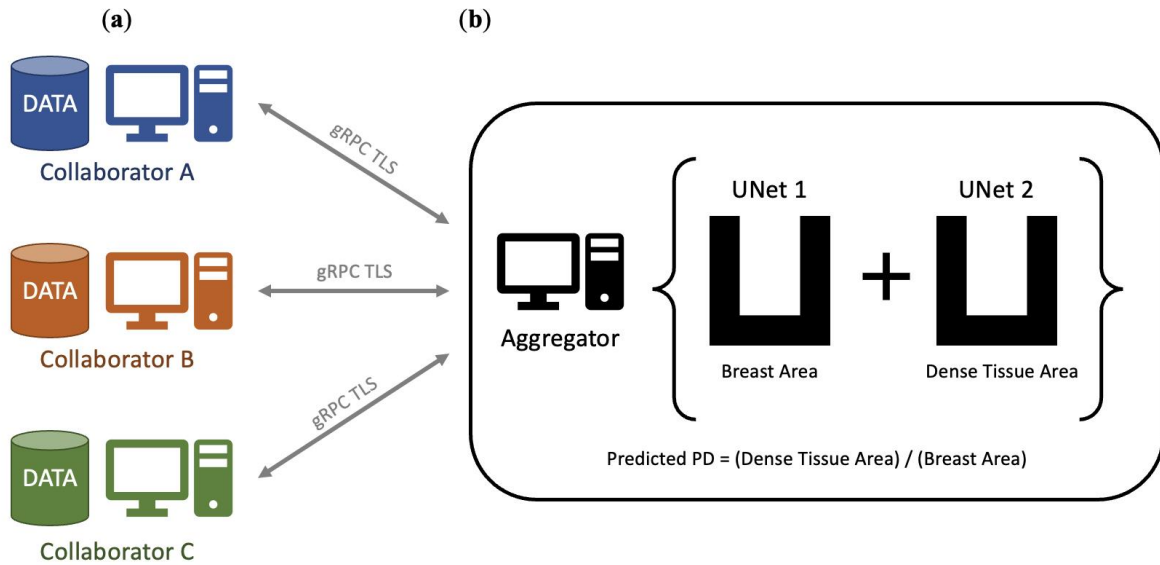


Fig. 1. System-level diagram of MammoDL. (a) Three collaborator nodes are shown, with each performing local training and then transferring the relevant tasks, model and optimizer weights, and other metrics to the aggregator node. (b) The aggregator node represents the two UNet architectures with ResNet34 encodings. Model/metric updates occur in the aggregator node, which train the model to execute segmentation of the breast and dense tissue based on information from all of the collaborators combined. After training is complete, a user can run inference on a new FFDM image to return a breast PD estimation and a spacial mapping that shows the dense tissue delineated from the non-dense tissue.

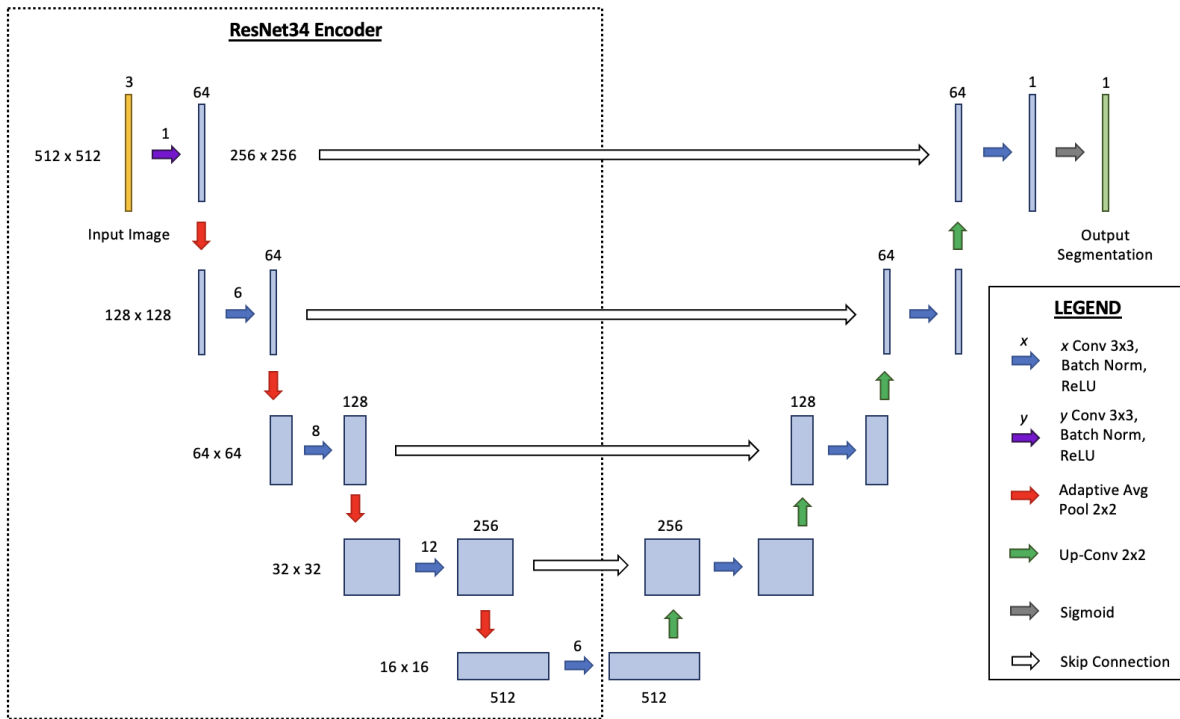


Fig. 2. Diagram of UNet with ResNet34 encoder. The left-hand portion of the UNet architecture corresponds to the “down-sampling” or “encoder” section, where the ResNet34 leverages 2×2 adaptive average pooling to progressively reduce the dimensions of the mammogram image while increasing the number of feature maps. The ResNet34 operates in five distinct blocks separated by pooling layers, the first corresponding to a single 7×7 convolutional layer with batch normalization and ReLU activation and the last four corresponding to 32 3×3 convolutional layers with batch normalization and ReLU activation. The last layer in the ResNet34 is typically a fully-connected classifier layer, which is omitted in this UNet architecture. The left-hand portion represents the “up-sampling” or “decoding” section, which involves mirror-like 2×2 up-convolution operations separating convolutional layers until the mammogram image returns to its original size, albeit with only a single channel.

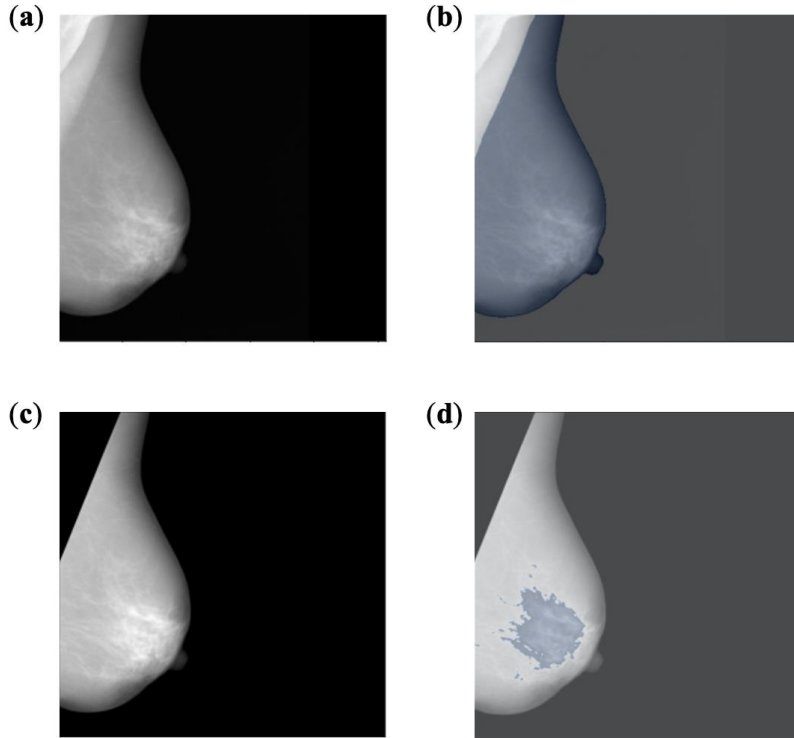


Fig. 3. Stages of the segmentation process in the MammoDL training pipeline. (a) This image shows an unprocessed FFDM in MLO-view from the HUP dataset. (b) After pre-processing, which includes removal of the metal tag, normalization to $[0, 255]$, down-sampling to 512×512 , and adjustment of contrast, the first UNet segments the breast from all other parts of the FFDM image, including the background and pectoralis muscle. Some data augmentation does occur at this stage, limited to flips across the x- and y-axis. (c) The background and pectoralis muscle are removed from the image entirely. Since the initial image was in MLO-view, the absence of the pectoralis muscle is noticeable. The area (i.e., number of pixels) corresponding to the breast is returned. (d) The second UNet delineates the dense tissue from the non-dense tissue. The area corresponding to the dense tissue is returned. The output of the second segmentation task is divided by the output of the first segmentation task, representing the proportion of dense tissue detected in the FFDM image. This value is returned as a percentage.

Dataset Type	Training and Validation		Test	
	MC	HUP	MC	HUP
Institution				
Number of Images	3,314	1,147	6463	278
Number of Women	1,662	575	414	110
Screening Start Date	2008	2010	2008	2011
Screening End Date	2012	2014	2014	2014
White (%)	98	47	94	-
Black/Other (%)	2	53	6	-

Table 1. General characteristics corresponding to the datasets. Each dataset is accompanied by its institution, the number of FFDM images present, the number of women in the screening cohort, the year that the screening began, the year that the screening finished, the percent of white subjects present in the screening and the percent of black/other subjects present in the screening.

Although race information was not available for the test HUP subjects, it is known that the racial distribution of the cohort was similar to that of the diverse screening population at HUP [35].

Training Type	Training/Validation Data	Performance on MC Validation Data			Performance on HUP Validation Data		
		MAE (%)	Breast DSC	Dense DSC	MAE (%)	Breast DSC	Dense DSC
Federated	HUP + MC	3.9740	0.9880	0.7634	4.2811	0.9727	0.6787
Centralized	HUP	13.3893	0.9545	0.0037	9.0138	0.9766	0.2732
Centralized	MC	21.4865	0.9865	0.4162	13.8530	0.1389	0.1895
Centralized	HUP + MC	3.7918	0.9896	0.7755	3.9711	0.9813	0.7078

Table 2. Performance on development validation dataset using federated versus centralized training. As expected, the models trained on both the HUP and MC data perform better than those trained on single-institution datasets, which provides strong motivation for the need for multi-institutional collaboration in ML-based medical imaging. The performance of the federated training scheme closely approaches that of the centralized one, model But the centralized training scheme presents numerous privacy and ownership concerns, while maintaining the privacy of patient mammogram data. Therefore, the federated learning pipeline represents a crucial addition to breast PD estimation tools in order to ensure generalization performance is maximized.

Training Type	Development Data	Performance on MC Test Data			Performance on HUP Test Data		
		MAE (%)	Breast DSC	Dense DSC	MAE (%)	Breast DSC	Dense DSC
Federated	HUP + MC	3.9586	0.9881	0.7637	4.2409	0.9686	0.6417
Centralized	HUP	12.2529	0.8245	0.0060	6.8729	0.9625	0.3523
Centralized	MC	27.4804	0.9827	0.3815	11.2794	0.3954	0.3210
Centralized	HUP + MC	3.8616	0.9900	0.7745	3.9937	0.9722	0.6879

Table 3. Performance on test dataset using federated versus centralized training. The trend seen in Table 2 is replicated here.

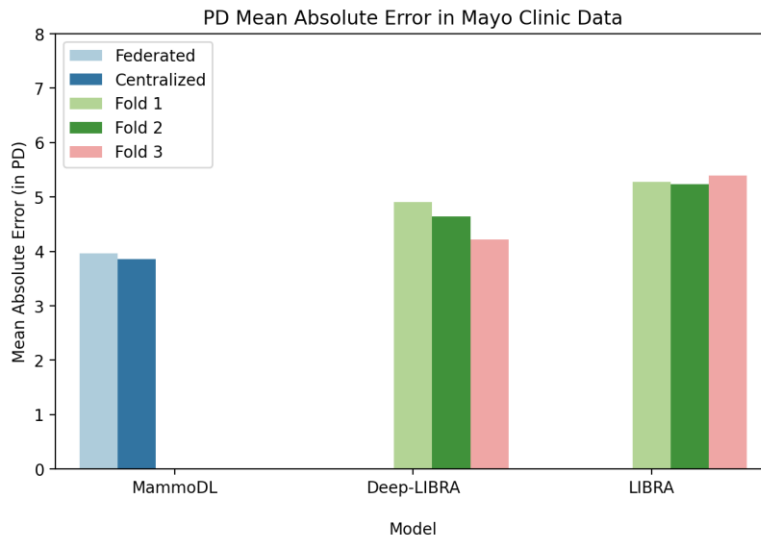


Fig. 4. Generalization performance of MammoDL in comparison to other breast PD estimation tools. This bar plot illustrates the testing accuracy exhibited by MammoDL, Deep-LIBRA, and LIBRA. The y-axis represents the MAE with respect to the the “gold-standard” Cumulus PD values. The bars for Deep-LIBRA and LIBRA represent the 3 reported cross-validation folds in the Deep-LIBRA paper [9]. MammoDL has two bars, the former representing the performance of the federated model and the latter showing the results of the centralized model (Table 3). All 3 models were tested on data from the Mayo Clinic, although the test dataset consisted of different images for MammoDL. The generalization behavior of the federated and centralized MammoDL models are better than those of both Deep-LIBRA and LIBRA.